Supporting Information

Exploring Attached-Buffer Effects and Gibbs-Donnan Equilibria in Ionomeric Energy-Transduction Materials

Lillian K. Hensleigh[1,2], Daiki Nishiori[1,2], Ian D. Peterson[1,2], and Gary F. Moore[*1,2]

[1]School of Molecular Sciences, Arizona State University, Tempe, AZ 85287-1604, United States

[2]Center for Applied Structural Discovery (CASD), The Biodesign Institute, Arizona State University, Tempe, AZ 85281, United States

gfmoore@asu.edu

Index

1. Experimental Methods

1.1. Materials

All compounds were synthesized from commercially available starting materials. Unless noted otherwise, all reagents were purchased from Sigma-Aldrich and used as received without further purification. Solvents were obtained from Fisher. Dimethylformamide was purified using a Vacuum Atmospheres Company (VAC) solvent purifier. Dichloromethane, hexanes, and methanol were distilled over appropriate drying agents before use.[1] All aqueous solutions were prepared using Milli-Q water (18.2 MΩ·cm). All reagents were purchased from commercial suppliers and used as received without further purification. The catalyst cobalt(II) 2,9,16,23-tetra-*tert*-butyl-29*H*,31*H* phthalocyanine (CoPc) was prepared via a cobalt insertion reaction (Scheme S1) with the commercially available metal-free (2,9,16,23-tetra-*tert*-butyl-29*H*,31*H* phthalocyanine) precursor (Pc) or purchased as a sublimed sample from April Scientific (AP-PC-051) that was used without further purification. Poly(*N*-vinylimidazole) (PVI) and poly(4-vinylpyridine) (PVP) were purchased from Polymer Source Inc. and Aldrich, respectively. Electrochemical analysis grade tetrabutylammonium hexafluorophosphate ($TBAPF_6$) electrolyte was obtained from Aldrich and stored in a desiccator containing calcium sulfate ($CaSO_4$) as a desiccant.

1.2. Instrumentation

Electrochemistry Measurements. All electrochemical experiments were performed using a Biologic SP-300 potentiostat and a conventional three-electrode cell at ambient temperature (20 ± 1 °C) under an atmosphere of argon (1 atm) or carbon dioxide (CO_2) (1 atm).

All data recorded using heterogenized CoPc samples were collected under hydrostatic conditions (*i.e.*, using stationary electrodes and no stirring of the electrolyte solution) using aqueous electrolyte conditions (0.1 M NaH_2PO_4) in a 260-ml five-neck electrochemical cell equipped with a 5-mm diameter glassy carbon working electrode with a surface area of 0.1963 cm^2 (Pine Research, AFED050P040GC) housed in a PTFE shroud (Pine Instruments, AFE5TQ050), a platinum coil counter electrode seated in a glass fritted isolation tube (Pine, AFCTR5) and a Ag/AgCl (4 M KCl) (Pine Research, RREF0021) reference electrode (where *E* vs the reversible hydrogen electrode (RHE) = *E* vs the standard hydrogen electrode (SHE) + 0.05916 V × pH = *E* vs Ag/AgCl + 0.05916 V × pH + 0.197 V was used to convert between the V vs Ag/AgCl, V vs SHE, and V vs RHE reference electrode scales).[2,3] The Nernst slope of 59.16 mV per pH unit, which is a theoretical value obtained at 25 °C (298.15 K), is used as a conversion factor. We note, however, that under the experimental conditions of 20 °C, the Nernst slope is 58.17 mV per pH unit. The resistance of the solution between a working electrode and the reference electrode (also called the uncompensated resistance, Ru) was determined using the zero internal resistance (ZIR) technique. To compensate for the solution resistance, the ZIR technique was performed before other experiments, and 85% of the uncompensated resistance was accounted for.

All data recorded using homogeneous CoPc samples were collected under hydrostatic conditions (*i.e.*, using stationary electrodes and no stirring of the solution) using a 15-ml electrochemical cell (BASi, 011504) equipped with a 3-mm glassy carbon working electrode with a surface area of 0.07 cm^2 (BASi, MF-2012), a platinum counter electrode, silver wire pseudoreference electrode, as well as PTFE inlet and outlet tubing (BASi, 010537) for sparging of the electrolyte solution. The potential of the silver wire pseudoreference electrode was determined by using the ferrocenium/ferrocene (Fc^+/Fc) redox couple as

an internal standard. The working electrode was cleaned between experiments by polishing with alumina (50 nm diameter) slurry (Allied High Tech Products Inc, 90-187505), followed by solvent rinses. Cyclic voltammograms were collected at a scan rate of 100 mV s^{-1}, under a constant stream of argon.

Mass Spectrometry. All Mass spectra were obtained using a Voyager DE STR matrix-assisted laser desorption/ionization time-of-flight (MALDI-TOF) mass spectrometer or Bruker microFlex LRF. All spectra were collected using positive ion mode and *trans*,*trans*-1,4-diphenyl-1,3-butadiene as a matrix.

Ultraviolet–Visible-Near-Infrared (UV–Vis-NIR) Spectroscopy. All UV–Vis-NIR spectra were recorded using a Shimadzu SolidSpec-3700 spectrometer with a deuterium (D_2) lamp for the ultraviolet range and a WI (halogen) lamp for the visible and near-infrared.

Gas Fourier Transform Infrared Spectroscopy. Gas Fourier transform infrared spectroscopy was performed using a Temperature Controlled Gas Cell (TCG-3-XXX) accessory (**Figure S1b**) with KBr optical windows in a Vertex 70 Fourier Transform Infrared (FTIR) spectrometer (Bruker). Spectra were collected in transmission mode with a resolution of 0.5 cm^{-1} using 128 scans, a dry nitrogen purge, a GloBar MIR source, a broadband KBr beamsplitter, and a liquid nitrogen-cooled MCT detector. Background measurements (also collected using 128 scans) were obtained using the gas analysis cell following

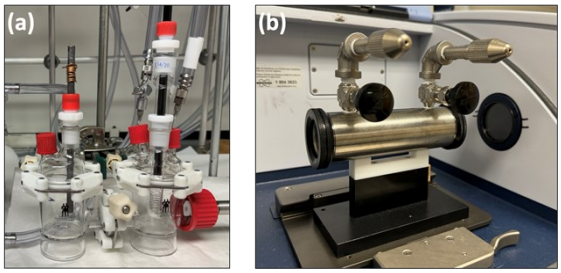

Figure S1. Photos of **(a)** a customized electrochemical cell and **(b)** a customized Fourier transform infrared (FTIR) spectroscopy cell used for analysis of gas phase head-space samples.

sparging with argon, and all data were processed using OPUS software. Following polarization, a 5-ml aliquot of headspace gas was removed and injected using a gastight syringe (Hamilton, 81420) into a custom gas FTIR cell and analyzed to quantify gas products. The carbon monoxide (CO) signal was confirmed using lecture bottles of standard calibration gases containing CO and nitrogen (N_2) mixtures of 1%, 5%, 10%, and 20% CO in N_2 (MESA Specialty Gases & Equipment). A calibration curve showing the CO signal intensity versus CO concentration (see **Figure S13**) was prepared by measuring the signal intensity of the CO peak observed at 2172.8 cm^{-1} (within the 0.5 cm^{-1} resolution of our measurements), and recorded using a 5-ml sample of headspace gas following injection of 5 ml of each of the standard CO calibration gases into the custom electrochemical cell (see **Figure S1a**) and 30 minutes of equilibration with electrolyte solution. In all gas product analyses, the working, and counter electrodes were housed in opposite chambers of the custom electrochemical cell which are separated by a Nafion (117) membrane. The working electrode was a glassy carbon disk electrode (Pine Research, AFED050P040GC) housed in a PTFE shroud (Pine Instruments, AFE5TQ050), the counter electrode was a graphite rod (Pine, MPGRR250), and the reference electrode was Ag/AgCl (4 M KCl) (Pine Research, RREF0021) and was positioned in the chamber containing the working electrode. In all gas product detection experiments, electrolyte was pre-sparged with argon for 30 minutes and 50 ml was transferred to each chamber of the electrochemical cell via cannula prior to carrying out controlled potential electrolysis.

Gas Chromatography. Confirmation of hydrogen (H_2) generation was performed via gas chromatography using an Agilent 490 Micro gas chromatograph equipped with a 5 Å MolSieve column at a temperature of 80 °C and argon as the carrier gas. Gas samples were syringe-injected using 5-ml aliquots of headspace gas collected with a gastight Hamilton syringe from a sealed electrochemical (EC) cell. Before the experiment, the EC cell was purged for 30 minutes with argon and 5 ml of headspace gas was analyzed to confirm the absence of CO and H_2. Following polarization, an additional 5-ml aliquot of headspace gas was removed and analyzed to quantify gas products. The H_2 retention time was confirmed using lecture bottles of standard calibration gases containing H_2 and N_2 mixtures of 0.01%, 1%, 5%, and 10% H_2 in N_2 (MESA Specialty Gases & Equipment). A calibration curve was prepared (see **Figure S14**) by recording the area of the H_2 signal of a 5-ml sample of headspace gas following injection of 5 ml of each of the standard H_2 calibration gases into the custom electrochemical cell (see **Figure S1a**) and 30 minutes of equilibration with the electrolyte solution. In all gas product analyses, the working and counter electrodes are housed in opposite chambers of the custom EC cell which are separated by a Nafion (117) membrane. The working electrode was a glassy carbon disk electrode (Pine Research, AFED050P040GC) housed in a PTFE shroud (Pine Instruments, AFE5TQ050), the counter electrode was a graphite rod (Pine, MPGRR250), and the reference electrode was Ag/AgCl (4 M KCl) (Pine Research, RREF0021) and was positioned in the chamber containing the working electrode. In all gas product detection experiments, electrolyte was pre-sparged with argon for 30 minutes and 50 ml was transferred to each chamber of the electrochemical cell via cannula prior to carrying out controlled potential electrolysis.

Ultraviolet–visible-near-infrared spectroelectrochemistry (UV–Vis-NIR-SEC) measurements. All UV−Vis-NIR-SEC measurements performed using a Biologic SP-200 potentiostat, a Pt honeycomb working electrode (Pine, AB01STC1PT), a Pt counter electrode, and a silver wire pseudoreference electrode. In all experiments, the supporting electrolyte contained 0.1 M $TBAPF_6$ and was sparged with argon (30 min). Thin layer constant potential electrolysis was monitored via UV−Vis-NIR as the working electrode was polarized in a stepwise manner (*i.e.*, an incrementally increasing bias potential versus the silver wire reference). Before changing the electrode polarization, absorption spectra were continuously collected at each applied potential until there were no significant changes in the resulting absorption spectra. This procedure was repeated until increasing the polarization no longer resulted in significant changes between UV−Vis-NIR spectra collected prior to and following the potential step. The Pt honeycomb electrode was cleaned between experiments by collecting cyclic voltammograms in 0.1 M H_2SO_4, followed by rinsing with 18.2 MΩ cm water and then acetone.

1.3. Synthesis of cobalt(II) 2,9,16,23-tetra-*tert*-butyl-29*H*,31*H* phthalocyanine

The catalyst cobalt(II) 2,9,16,23-tetra-*tert*-butyl-29*H*,31*H* phthalocyanine, abbreviated as CoPc, was prepared via a cobalt insertion reaction (**Scheme S1**) with the commercially available metal-free (2,9,16,23-tetra-*tert*-butyl-29*H*, 31*H* phthalocyanine) precursor (Pc). MALDI-TOF mass spectrometry results indicate an increase in mass of the precursor consistent with the addition of a single cobalt.

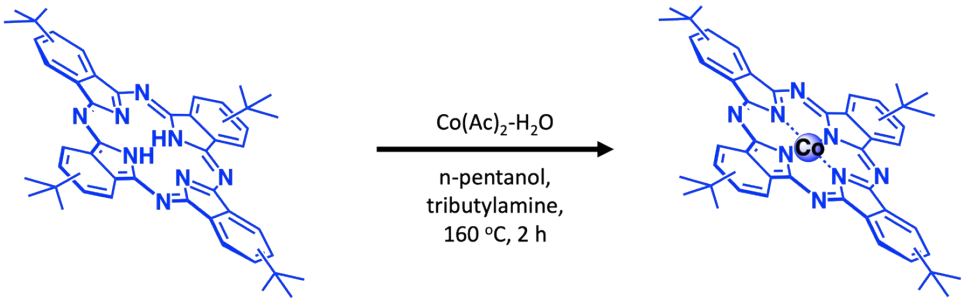

Scheme S1. Synthetic scheme for preparing cobalt(II) 2,9,16,23-tetra-*tert*-butyl-29*H*,31*H* phthalocyanine.

1.4. Characterization of cobalt(II) 2,9,16,23-tetra-*tert*-butyl-29*H*,31*H* phthalocyanine

1.4.1. MALDI-TOF

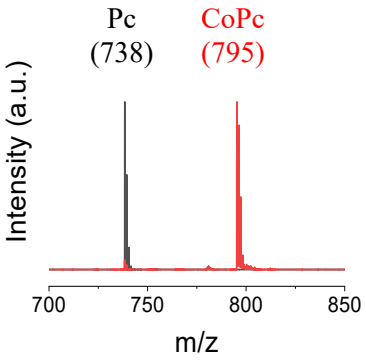

Figure S2. MALDI-TOF mass spectra of 2,9,16,23-tetra-*tert*-butyl-29*H*,31*H* phthalocyanine (black) or 2,9,16,23-tetra-*tert*-butyl-29*H*,31*H* phthalocyanine (red) recorded using *trans*,*trans*-1,4-diphenyl-1,3-butadiene as a matrix.

1.4.2. UV-Vis

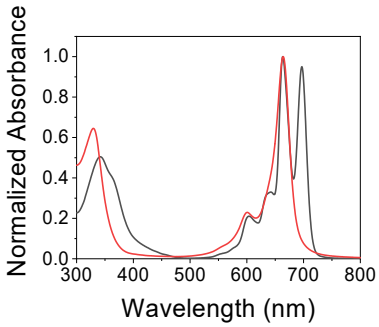

Figure S3. UV-Vis spectra of 2,9,16,23-tetra-*tert*-butyl-29*H*,31*H* phthalocyanine dissolved in *N,N'*-dimethylformamide (8 μM) (black) and cobalt(II) 2,9,16,23-tetra-*tert*-butyl-29*H*,31*H* phthalocyanine dissolved in *N,N'*-dimethylformamide (10 μM) (red). All spectra were recorded at room temperature using a quartz cuvette with a 1 cm pathlength.

1.4.3. Electrochemical Data

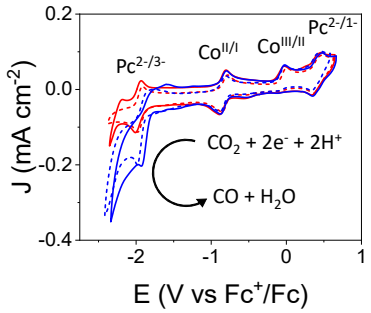

Figure S4. Cyclic voltammograms recorded using cobalt(II) 2,9,16,23-tetra-*tert*-butyl-29*H*,31*H* phthalocyanine (0.34 mM) dissolved in *N,N'*-dimethylformamide containing tetrabutylammonium hexafluorophosphate (0.1 M) as a supporting electrolyte, under argon (1 atm) (red) or CO_2 (1 atm) (blue), and in the absence (dash) or presence (solid) of trifluoroethanol (0.1 M) as a proton donor. All voltammograms were recorded at a scan rate of 100 mV s^{-1} using a glassy carbon working electrode and ferrocenium/ferrocene as an internal standard. The most positive couple under argon is assigned to a ring reduction/oxidation process ($Pc^{2-/1-}$). This is followed by an electrochemically and chemically irreversible couple at more negative potentials assigned to a cobalt centered ($Co^{III/II}$) process. The next most cathodic couple is assigned to another cobalt centered redox process ($Co^{II/I}$) that is followed by a phthalocyanine ligand-based redox process ($Pc^{2-/3-}$). These assignments are consistent with previously reported redox couples for CoPc in organic conditions.[4–7]

Table S1: Potentials of Homogeneous CoPc[a]

	E_{pa} (V vs Fc^+/Fc)	E_{pc} (V vs Fc^+/Fc)	ΔE_p (V)	$(E_{pa} + E_{pc})/2$ (V vs Fc^+/Fc)
$[Co^{I}Pc]^{-}/[Co^{I}Pc]^{2-}$	-1.91	-1.98	0.065	-1.95
$[Co^{II}Pc]^{0}/[Co^{I}Pc]^{-}$	-0.80	-0.89	0.086	-0.85
$[Co^{III}Pc]^{+}/[Co^{II}Pc]^{0}$	0.0067	-0.12	0.12	-0.055
$[Co^{III}Pc]^{2+}/[Co^{III}Pc]^{+}$	0.48	0.36	0.12	0.42

[a]Reported potentials were obtained from data in **Figure S4**

1.4.4. Spectroelectrochemistry

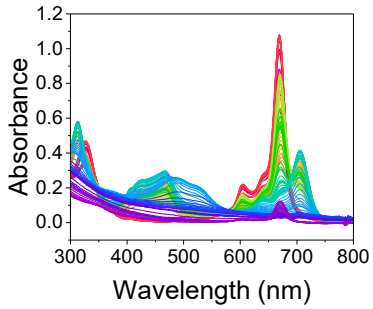

Figure S5. Spectra recorded using UV-Vis-NIR spectroelectrochemical techniques (see Section 1.2 on Instrumentation) and a sample of cobalt(II) 2,9,16,23-tetra-*tert*-butyl-29*H*,31*H* phthalocyanine (CoPc) dissolved in in dichloromethane (0.05 mM) containing tetrabutylammonium hexafluorophosphate (0.1 M) as a supporting electrolyte. The spectra were recorded at applied potentials sufficient to generate the one-electron reduced complex $[Co^{I}Pc]^{-}$ (the dominant species in the yellow-colored spectrum), and the two-electron reduced complex $[Co^{I}Pc]^{2-}$ (the dominant species in the green-colored spectrum).

1.5 Determination of Binding Constants

Binding constants of cobalt(II) 2,9,16,23-tetra-*tert*-butyl-29*H*,31*H* phthalocyanine (CoPc) with either *N*-methylimidazole (*N*-MeIm) or 4-vinylpyridine (4-MePy) were measured using electrochemical methods (cyclic voltammetry) that quantify shifts in the formal potential of the Co(II)Pc/Co(I)Pc redox couple upon varying the bulk concentration of *N*-MeIm or 4-MePy in the electrolyte solutions. The values of these binding constants guided our selection of the ~1:3800 ratio of CoPc to total polymer functional group sites to 1) diminish the presence of non-coordinated catalysts within the CoPc|PVP and CoPc|PVI assemblies as well as 2) minimize the competition between the coordination of catalysts versus protonation of the polymer functional group sites upon exposure to aqueous electrolyte solutions.

In these experiments, aliquots of solutions containing varying concentrations (1 mM to 1 M) of either 4-MePy or *N*-MeIm dissolved in DMF containing CoPc (0.1 mM) and $TBAPF_6$ (0.1 M) as the supporting electrolyte were added to a 10-ml solution of CoPc (0.1 mM) in DMF containing $TBAPF_6$ (0.1 M) as the supporting electrolyte to yield the total ligand concentrations indicated on the x-axis of plots shown in **Figure S7**. This approach keeps the concentration of CoPc at a constant concentration of 0.1 mM while varying the concentration of the 4-MePy or *N*-MeIm ligands. As an example, the equilibrium involving Co(II)Pc-*N*-MeIm, Co(I)Pc, and *N*-MeIm, is represented by the reduction half reaction shown in **eq S1**:

$$Co(II)Pc - N - MeIm + e^{-} \rightleftharpoons Co(I)Pc + N - MeIm$$
$$E^{o}_{ligand-coupled\ reduction\ half\ reaction} = X\ V\ vs\ a\ reference\ potential\ scale, \qquad \text{eq S1}$$

where $E^{o}_{ligand-coupled\ reduction\ half\ reaction}$ is the standard potential of the ligand-coupled half reaction indicated in **eq S1** (with units of V vs a reference electrode potential).

When the electrons required to drive this half reaction are supplied by a reference electrode (or other electron donor) the oxidation half reaction can be expressed as follows:

$$reference\ electron\ donor \rightleftharpoons reference\ electron\ acceptor + e^-$$
$$E^{o}_{reference\ oxidation\ half\ reaction} = X\ V\ vs\ a\ reference\ potential\ scale, \quad \text{eq S2}$$

where $E^{o}_{reference\ oxidation\ half\ reaction}$ is the standard potential of the oxidation half reaction expressed in **eq S2** (with units of V vs a reference electrode potential). When the reference electrode potentials is the same as the reference oxidation half reaction, $E^{o}_{reference\ oxidation\ half\ reaction}$ will—by definition—be equal to zero 0 V vs the reference electrode potential.

Combining **eq S1** and **eq S2** yields the overall redox reaction shown in **eq S3**:

$$Co(II)Pc - N - MeIm + reference\ electron\ donor \rightleftharpoons Co(I)Pc + N - MeIm + reference\ electron\ acceptor$$

$$E^{o}_{cell\ overall} = E^{o}_{ligand-coupled\ reduction\ half\ reaction} + E^{o}_{reference\ oxidation\ half\ reaction} = \frac{\Delta G^{o}_{overall}}{-nF}, \quad \text{eq S3}$$

where $E^{o}_{cell\ overall}$ is the standard potential of the overall cell reaction indicated in **eq S3** (with units of V), $\Delta G^{o}_{overall}$ is the related standard Gibbs free energy of the overall cell reaction (with units of J mol^{-1}), n is the number of electrons transferred per reaction, (where n = 1 for the one-electron $Co^{II/I}$ redox couple), and F is the Faraday constant (96,485.3321 C mol^{-1}).

The overall cell reaction indicated in **eq S3** is a ligand-coupled electron transfer reaction that can be conceptually deconvoluted into an electron transfer reaction and a ligand-binding reaction, as indicated in **eq S4** and **eq S5**, respectively,

$$Co(II)Pc + reference\ electron\ donor \rightleftharpoons Co(I)Pc + reference\ electron\ acceptor$$
$$\Delta G^{o}_{pure\ ET} = -nFE^{o}_{cell\ pure\ ET}, \quad \text{eq S4}$$

where $\Delta G^{o}_{pure\ ET}$ is the standard Gibbs free energy of the electron transfer reaction indicated in **eq S4** (with units of J mol^{-1}) and $E^{o}_{cell\ pure\ ET}$ is the related standard cell potential of the electron transfer reaction (with units of V), and

$$Co(II)Pc - N - MeIm \rightleftharpoons CoPc + N - MeIm$$
$$\Delta G^{o}_{ligand\ binding} = -RTln[K], \quad \text{eq S5}$$

where $\Delta G^{o}_{ligand\ binding}$ is the standard Gibbs free energy of the ligand-binding indicated in **eq S5** (with units of J mol^{-1}), and the related binding constant, *K*, is expressed as follows in **eq S6**:

$$K = \frac{[Co(I)Pc][N-MeIm]}{[Co(II)-N-MeIm]}$$
eq S6

Using Hess law,[8] summation of the standard Gibbs free energies of the electron-transfer reaction (see **eq S4**) and ligand-binding reaction (see **eq S5**) yields the re-expression of the standard Gibbs free energy for the overall ligand-coupled electron transfer reaction (**eq S3**), $\Delta G^{o}_{overall}$, as indicated in **eq S7**:

$$\Delta G^{o}_{overall} = \Delta G^{o}_{pure\ ET} + \Delta G^{o}_{ligand\ binding} \quad \text{eq S7}$$

Combining **eq S7** with **eq S4** and **eq S5**, and using the Nernst relationship to substitute $\Delta G^{o}_{overall}$ with $-nFE^{o}_{cell\ overall}$ and $\Delta G^{o}_{pure\ ET}$ with $-nFE^{o}_{cell\ pure\ ET}$, yields **eq S8**:

$$E^{o}_{cell\ overall} = E^{o}_{cell\ pure\ ET} + \frac{RT}{nF} ln[K] \quad \text{eq S8}$$

where R is the universal gas constant (8.314 J mol^{-1} K^{-1}) and T is the temperature (298.15 K).

Using the Nernst relationship to account for non-standard conditions, **eq S8** can be re-expressed in terms of a formal potential ($E^{o'}_{cell\ overall}$), rather than the standard potential, to yield **eq S9**:

$$E^{o'}_{cell\ overall} = (E^{o}_{cell\ pure\ ET} + \frac{RT}{nF} ln[K]\ ) + (\ -\frac{RT}{nF} ln[Q_r]) \quad \text{eq S9}$$

where Q_r is the reaction quotient expressed in **eq S10**.

$$Q_r = \frac{[Co(I)Pc][N-MeIm]}{[Co(II)-N-MeIm]}$$
eq S10

Converting to the natural log terms in **eq S9** to base 10 log terms and substituting in the values R, T, and F, yields **eq S11**.

$$E^{o'}_{cell\ overall} = (E^{o}_{cell\ pure\ ET} + 0.05916\ log[K]) - 0.05916\ log[N-MeIm] \quad \text{eq S11}$$

When $E^{o'}_{cell\ overall}$ and $E^{o}_{cell\ pure\ ET}$ are reported versus the same reference electrode potential scale the reference electrode terms will cancel, and **eq S11** can be expressed in terms of half reaction potentials, rather than cell potentials, as indicated in **eq S12**.

$$E^{o'}_{ligand-coupled\ reduction\ half\ reaction} = (E^{o}_{pure\ ET\ reduction\ half\ reaction} + 0.05916\ log[K]) - 0.05916\ log[N-MeIm],$$

eq S12

Where $E^{o'}_{ligand-coupled\ reduction\ half\ reaction}$ is the formal half-reaction potential of the reaction indicated in **eq S1** under non-standard concentrations of *N*-MeIm and $E^{o}_{pure\ ET\ reduction\ half\ reaction}$ is the standard half-reaction potential as expressed in **eq 13**.

$$Co(II)Pc + e^- \rightleftharpoons Co(I)Pc$$
$$E^{o}_{pure\ ET\ reduction\ half\ reaction} = X\ V\ vs\ a\ reference\ potential\ scale$$

eq S13

In the context of the analysis used in this work, it is convenient to re-express **eq 12** in the linear form of y = mx + b shown in **eq S14**.

$$E^{o'}_{ligand-coupled\ reduction\ half\ reaction} = -0.05916 \log[N-MeIm] + (E^{o}_{pure\ ET\ reduction\ half\ reaction} + 0.05916\ log[K])$$

eq S14

The standard potential of the pure electron transfer reduction half reaction, $E^{o}_{pure\ ET\ reduction\ half\ reaction}$, can be estimated from voltammetry measurements of the Co(II)Pc/Co(I)Pc midpoint potential ($E_{1/2}$) recorded in the absence of *N*-MeIm (see **Figure S4** and **Figure S6**). The standard potential of the ligand-coupled reduction half reaction, $E^{o}_{ligand-coupled\ reduction\ half\ reaction}$, (see **eq S12**) and the related binding constant, *K*, (see **eq S6**) can be determined from voltammetry measurements of the Co(II)Pc/Co(I)Pc $E_{1/2}$ recorded in the presence of varying concentrations of *N*-MeIm (see **Figure S6** and **Figure S7**) and using the data to generate $E_{1/2}$ vs log[*N*-MeIm] plots.

For the work reported herein, the resulting $E_{1/2}$ vs log[*N*-MeIm] plots (see **Figure S7**) yielded a slope of -0.059 ± 0.004 V dec^{-1} (consistent with a one-ligand binding/unbinding per one-electron transfer and in accordance with the Nernst relationship, where the half-cell potential should change by 0.5916 mV per 10-fold change in the activity of the ligand). Extrapolation to the y-intercept yields a Co(II)Pc/Co(I)Pc $E_{1/2}$ value at a ligand concentration of 1 M that thus approximates $E^{o}_{ligand-coupled\ reduction\ half\ reaction}$ and yields a related *K* value for CoPc binding with *N*-MeIm (see **eq S14**). A similar analysis was used to determine the binding constant of CoPc with 4-methylpyridine (4-MePy), by replacing [*N*-MeIm] with [4-MePy] (see **Figure S6** and **Figure S7**).

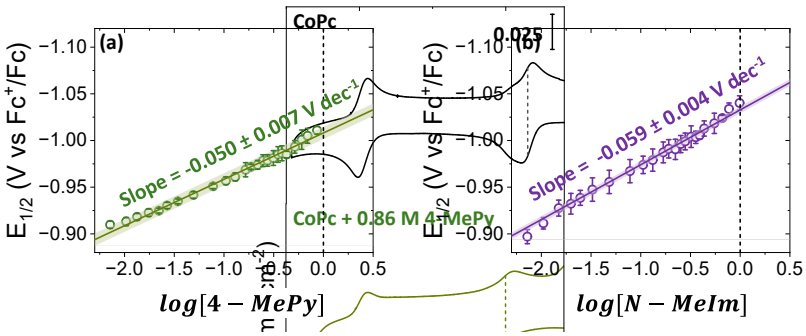

Figure S7. $Co^{II/I}$ midpoint potential ($E_{1/2}$) vs the log of the concentration of **(a)** the ligand 4-methylpyridine (green) or **(b)** the ligand *N*-methylimidazole (purple). In both plots, the indicated slopes are the average slope obtained from three separate experiments, the shaded areas represent the standard deviations from the mean values, and the error bars represent the standard deviation of triplicate data points. The slopes obtained from these plots yield information on ligand binding and unbinding stoichiometry per electron transferred (where, per the Nernst relationship, the half-cell potential should change by 59.16 mV per 10-fold change in the activity of the ligand). The y-intercepts obtained from these plots yield information on the binding constants (*K*) between CoPc and the indicated ligand (see the relationship given in eq S14). The value of $E_{1/2}$ at a ligand concentration of 1 M yields an estimate of the standard potential of the ligand-coupled reduction half reaction ($E^{o}_{ligand-coupled\ reduction\ half\ reaction}$) (see eq S12).

Figtetrabutylammonium hexafluorophosphate (0.1 M) as a supporting electrolyte in the absence of ligand (black), the presence of the ligand 4-methylpyridine (0.86 M) (green), or the presence of the ligand *N*-methylimidazole (1.0 M) (purple). All voltammograms were recorded at a scan rate of 100 mV^{-1}, under argon (1 atm) and the vertical dashed lines indicate the average of the anodic and cathodic peaks of the $Co^{II/I}$ couple.

Using the relationship given in **eq S14** and the data shown in **Figure S6** and **Figure S7** yields the $E^{o}_{pure\ ET\ reduction\ half\ reaction}$, $E^{o}_{ligand-coupled\ reduction\ half\ reaction}$, and *K* values indicated in **Table S2** for CoPc binding with 4-MePy or *N*-MeIm.

Table S2. Values of $E^{o}_{pure\ ET\ reduction\ half\ reaction}$, $E^{o}_{ligand-coupled\ reduction\ half\ reaction}$, and the binding constant, *K*[a]

	4-MePy	*N*-MeIm
$E^{o}_{pure\ ET\ reduction\ half\ reaction}$ **(V vs Fc^+/Fc)**	-0.85	-0.85
$E^{o}_{ligand-coupled\ reduction\ half\ reaction}$ **(V vs Fc^+/Fc)**	-1.008 ± 0.009	-1.03 ± 0.01
Ligand Binding Constant, *K*	(5 ± 2) x 10^2	(14 ± 6) x 10^2

(M^{-1})

[a]The binding constant, *K*, was determined using the data in **Figure S7**

1.6 Preparation of Electrode Coatings

All electrode coatings were prepared so the total number pyridyl or imidazolyl units deposited onto each electrode is 9.5 x 10^{-7} moles (yielding a per-geometric area pyridyl-site or imidazolyl-site loading of 4.8 x 10^{-6} mol cm^{-2}) and the total number of cobalt(II) 2,9,16,23-tetra-*tert*-butyl-29*H*,31*H* phthalocyanine (CoPc) units is 2.5 x 10^{-10} moles (yielding a CoPc per-geometric area loading of 1.3 nmol cm^{-2}). Thus, the ratio of CoPc units to pyridyl units in CoPc|PVP is ~1:3800 and the ratio of CoPc units to imidazolyl units in CoPc|PVI is also ~1:3800.

With the aim of reducing variations in the per-geometric area loading of catalysts across the heterogenized samples, we used the *tert*-butyl-group-containing cobalt phthalocyanine to 1) improve solubility and avoid aggregation in the homogeneous DMF solutions used for depositing the electrode coatings and 2) enhance hydrophilic-hydrophobic interactions when suspending the polymer-encapsulated CoPc units in aqueous solutions. Further, the solutions used for depositing the electrode coatings were prepared using stock solutions of CoPc in DMF (25 μM) that were sonicated for 15 minutes and that yielded an absorbance of 0.87 at 669 nm following a 4-fold dilution of the stock solution. The selection of glassy carbon as a solid-state support for preparing the chemically-modified working electrodes reported herein facilitates comparisons to other published reports on using polymer-immobilized cobalt phthalocyanines.[9–11] Carbon electrodes also provide sufficient electrical conductivity, chemical inertness, and stability over the range of potentials used in this work for investigating the electrochemical reduction of CO_2.[7,12–17]

The solutions used to produce the CoPc|PVP-modified electrodes were prepared by adding a portion of the CoPc stock solution to a 1-ml volumetric flask containing 10.0 mg of PVP to achieve a total solution volume of 1 ml that is 25 μM in CoPc and 95.1 mM in pyridyl units. This solution, containing CoPc and PVP, was used to prepare CoPc|PVP-modified electrodes by depositing 10.0 μL of the solution onto the electrodes followed by drying in an oven (Thermo Scientific VWR Vacuum Oven, Model 6290, VWR catalog number 89508-426) at a temperature of 70 °C for 15 min. **Eq S15** indicates the relationship used for determining the moles of pyridyl units deposited on the CoPc|PVP-modified electrodes

$$moles\ of\ pyridyl\ units\ deposited = \frac{Mass\ PVP\ in\ stock\ solution\ (g)}{molar\ mass\ of\ vinyl\ pyridine\ (\frac{g}{mol})} \times \frac{volume\ of\ stock\ solution\ deposited\ (\mu L)}{total\ volume\ of\ stock\ solution\ (\mu L)}$$

$$= \frac{0.0100\ g}{105.14\ \frac{g}{mol}} \times \frac{10.0\ \mu L}{1000\ \mu L} = 9.51\ \times\ 10^{-7}\ mol\ of\ pyridyl\ units$$

eq S15

The solutions used to produce the CoPc|PVI-modified electrodes were prepared by adding a portion of the CoPc stock solution to a 1-ml volumetric flask containing 8.9 mg of PVI to achieve a total solution

volume of 1 ml that is 25 µM in CoPc and 95 mM in imidazolyl units. This solution, containing CoPc and PVI, was used to prepare CoPc|PVI-modified electrodes by depositing 10 µL of the solution onto the electrodes followed by drying in an oven (Thermo Scientific VWR Vacuum Oven, Model 6290, VWR catalog number 89508-426) at a temperature of 70 °C for 15 min. **Eq S16** indicates the relationship used for determining the moles of pyridyl units deposited on the CoPc|PVP-modified electrodes:

$$moles\ of\ imidazolyl\ units\ deposited = \frac{Mass\ PVI\ in\ stock\ solution\ (g)}{molar\ mass\ of\ vinyl\ imidazole\ (\frac{g}{mol})} \times \frac{volume\ of\ stock\ solution\ deposited\ (\mu L)}{total\ volume\ of\ stock\ solution\ (\mu L)}$$

$$= \frac{0.0089\ g}{94.11\ \frac{g}{mol}} \times \frac{10.0\ \mu L}{1000\ \mu L} = 9.5\ \times\ 10^{-7}\ mol\ of\ imidazoyl\ units.$$

eq S16

Eq S17 indicates the relationship used for determining the moles of CoPc units deposited on the CoPc|PVP-modified electrodes and the CoPc|PVI-modified electrodes.

$$moles\ of\ CoPc\ units\ deposited = \frac{Mass\ CoPc\ in\ stock\ solution}{molar\ mass\ of\ CoPc} \times \frac{volume\ of\ stock\ solution\ deposited}{total\ volume\ of\ stock\ solution}$$

$$= \frac{0.000020\ g}{795.88\frac{g}{mol}} \times \frac{10\ \mu L}{1000\ \mu L} = 2.5\ \times\ 10^{-10}\ mol\ of\ CoPc$$

eq S17

1.7 Estimations of the Percentage of Polymer-Coordinated CoPc Units in the PVP and PVI Electrode Coatings

Using the experimentally determined binding constant of (5 ± 2) x 10^2 M^{-1} for the reaction of Co(II)Pc − 4-MePy ⇌ Co(II)Pc + 4-MePy, the equilibrium concentrations of polymer-coordinated CoPc in the solutions used to produce the CoPc|PVP-modified electrodes (see **eq S18**) were estimated using the values indicated in the **Table S3** and the relationship given in **eq S19**.

$$Co(II)Pc - pyidyl\ unit \rightleftharpoons Co(II)Pc + pyridyl\ unit$$

eq S18

Table S3. An "ICE table" used for approximating the equilibrium concentrations of CoPc-pyridyl units in the solutions used to produce the CoPc|PVP-modified electrodes

	[CoPc units] (M)	[pyridyl units] (M)	[CoPc-pyridyl units] (M)
Initial	2.5 x 10^{-5}	9.51 x 10^{-2}	0
Change	–x	–x	x
Equilibrium	2.5 x 10^{-5} – x	9.51 x 10^{-2} – x	x

$$K = \frac{[CoPc - pyridyl\ units]}{[CoPc\ units][pyridyl\ units]} = \frac{(x)}{(2.5 \times 10^{-5} - x)(9.51 \times 10^{-2} - x)} \sim (5 \pm 2) \times 10^{2}$$

eq S19

where *K* is the equilibrium constant of the reaction indicated in **eq S19**, and solving for x yields a CoPc-pyridyl units equilibrium concentration of ~(2.45 ± 0.02) × 10^{-5} M.

The CoPc-pyridyl units equilibrium concentration is then used to estimate the percentage of polymer-coordinated CoPc units in the solutions used to produce the CoPc|PVP-modified electrodes via leveraging the relationship given in **eq S20**:

$$\%\ Coodinated\ CoPc\ in\ PVP = \frac{[CoPc - pyridyl\ units]}{[CoPc\ units]} * 100$$

$$\sim \frac{(2.45 \pm 0.02) \times 10^{-5}}{2.5 \times 10^{-5}} * 100 = 97.9 \pm 0.7\ \%.$$

eq S20

Using the experimentally determined binding constant of (14 ± 6) x 10^{2} for the reaction of Co(II)Pc − *N*-MeIm ⇌ Co(II)Pc + *N*-MeIm, the equilibrium concentration of polymer-coordinated CoPc in the solutions used to produce the CoPc|PVI-modified electrodes (see **eq S21**) was estimated using the values indicated in **Table S4** and the relationship given in **eq S22**.

$$Co(II)Pc - imidazolyl\ unit \rightleftharpoons Co(II)Pc + imidazolyl\ unit$$

eq S21

Table S4. An "ICE table" used for approximating the equilibrium concentrations of CoPc-imidazolyl units in the solutions used to produce the CoPc|PVI-modified electrodes

	[CoPc units] (M)	**[imidazolyl units] (M)**	**[CoPc-imidazolyl units] (M)**
Initial	2.5 x 10^{-5}	9.5 x 10^{-2}	0
Change	–x	–x	x
Equilibrium	2.5 x 10^{-5} – x	9.5 x 10^{-2} – x	x

$$K = \frac{[CoPc - imidazolyl\ units]}{[CoPc\ units][imidazolyl\ units]} = \frac{(x)}{(2.5 \times 10^{-5} - x)(0.095 - x)} \sim \times (14 \pm 6) \times 10^{2}$$

eq S22

where *K* is the equilibrium constant of the reaction indicated in **eq S21**, and solving for x yields a CoPc-imidazolyl units equilibrium concentration of ~(2.489 ± 0.009) × 10^{-5} M.

The CoPc-imidazolyl units equilibrium concentration is then used to estimate the percentage of polymer-coordinated CoPc units in the solutions used to produce the CoPc|PVI-modified electrodes via leveraging the relationship given in **eq S23**:

$$\%\ Coodinated\ CoPc\ in\ PVI = \frac{[CoPc - imidazolyl\ units]}{[CoPc\ units]} * 100$$

$$\sim \frac{(2.489\ \pm\ 0.009)\ \times\ 10^{-5}}{2.5\ \times\ 10^{-5}} * 100 =\ 99.2\ \pm 0.4\ \%$$

.

eq S23

1.8 Estimation of the Concentrations of Imidazoyl Units and Pyridyl Units in the PVP and PVI Polymers

As indicated in **eq S24** and **eq S25**, the concentrations of pyridyl units and imidazolyl units in the PVP and PVI polymers were estimated using the molecular weights of the corresponding monomers [*i.e.*, 105.14 g mol^{-1} for 4-vinylpyridine (VPy) and 94.11 g mol^{-1} for *N*-vinylimidazole (VIm)] and the densities of the corresponding monomers (0.975 g cm^{-3} for VPy and 1.039 g cm^{-3} for VIm), which are used in place of densities for PVP and PVI.

The concentration of monomeric units in PVP ([$pyridyl\ units$]) was calculated using **eq S24**:

$$[pyridyl\ units]\ in\ PVP = \frac{density\ PVP\ (\frac{g}{ml})}{molar\ mass\ VPy\ (\frac{g}{mol})} \sim \frac{density\ VPy\ (\frac{g}{ml})}{molar\ mass\ VPy\ (\frac{g}{mol})}$$

$$= \frac{0.975\ \frac{g}{ml}}{105.14\ \frac{g}{mol}} = 9.27\ M$$

.

eq S24

We note that a PVP density of 1.15 g cm^{-3} was reported by ChemicalBook.[18] Using this value yields a pyridyl unit concentration of 10.9 M for PVP.

The concentration of imidazolyl units in PVI ([$imidazolyl\ units$]) was calculated using **eq S25**:

$$[imidazolyl\ units]\ in\ PVI = \frac{density\ PVI\ (\frac{g}{ml})}{molar\ mass\ VIm\ (\frac{g}{mol})} \sim \frac{density\ VIm\ (\frac{g}{ml})}{molar\ mass\ VIm\ (\frac{g}{mol})}$$

$$= \frac{1.039\ \frac{g}{ml}}{94.11\ \frac{g}{mol}} = 11.04\ M.$$

eq S25

Given the densities of VPy and VIm used for estimating the concentrations of pyridyl units in PVP and the concentrations of imidazolyl units in PVI likely underestimates the densities of the pyridyl units in PVP and the imidazolyl units in PVI. From this perspective, the analysis presented herein provides a lower limit of the pyridyl unit and imidazolyl unit concentrations in the polymers. However, upon exposure to aqueous solutions, the influx of water and ions into the polymers can cause swelling of the polymer phase.[19–21]

1.9 Estimations of the Volume and Film Thickness of PVP and PVI Polymer Electrode Coatings

Given all electrode coatings were prepared so the total number pyridyl units or imidazolyl units deposited onto the electrodes is ~9.51 x 10^{-7} moles (see **Section 1.6 on the Preparation of Electrode Coatings**), the pyridyl unit and imidazolyl unit concentrations of 9.27 M and 11.04 M, respectively (see **Section 1.8 on the Estimation of the Concentrations of Imidazoyl Units and Pyridyl Units in the PVP and PVI Polymers**), enable an estimate of both the volume and film thickness of the PVP and PVI electrode coatings.

The volume of the PVP-based coatings used in this work is estimated using the relationship indicated in **eq S26**,

$$volume\ of\ PVP\ coating = \frac{\#\ of\ pyridyl\ units\ (mol)}{[pyridyl\ units]\ in\ PVP\ \left(\frac{mol}{cm^3}\right)}$$

$$= \frac{9.51 \times 10^{-7}\ mol}{9.27\ M\ \times (\frac{1\ L}{1000\ cm^3})} = 1.03 \times 10^{-4}\ cm^3.$$

eq S26

The film-thickness of the PVP-based coatings used in this work is estimated using the relationship indicated in **eq S27**,

$$film\ thickness\ of\ PVPcoatings = \frac{volume\ of\ PVP\ coating\ (cm^3)}{electrode\ surface\ area\ (cm^2)}$$

$$= \frac{1.03 \times 10^{-4}\ cm^3}{0.1963\ cm^2} = 5.22 \times 10^{-4}\ cm.$$

eq S27

The volume of the PVI-based coatings used in this work is estimated using the relationship indicated in **eq S28**.

$$volume\ of\ the\ PVI\ coating = \frac{\#\ of\ imidazolyl\ units\ (mol)}{[imidazolyl\ units]\ in\ PVI\left(\frac{mol}{cm^3}\right)}$$

$$= \frac{9.5 \times 10^{-7}\ mol}{11.04\ M\ \times \left(\frac{1\ L}{1000\ cm^3}\right)} = 8.6 \times 10^{-5}\ cm^3$$

eq S28

The film-thickness of the PVI-based coatings used in this work is estimated using the relationship indicated in **eq S29**.

$$film\ thickness\ of\ the\ PVI\ coating = \frac{volume\ of\ PVI\ coating\ (cm^3)}{electrode\ surface\ area\ (cm^2)}$$

$$= \frac{8.6 \times 10^{-5}\ cm^3}{0.1963\ cm^2} = 4.4 \times\ 10^{-4}\ cm$$

.

eq S29

1.10 Estimation of the Concentration of CoPc in the PVP and PVI Polymer Electrode Coatings

Given the CoPc per-geometric area loading of 1.3 nmol cm^{-2} (see **Section 1.6 on the Preparation of Electrode Coatings**)and the estimated PVP coating thickness of 5.22 μm (see **eq S27**), the concentration of CoPc in the PVP coatings (*i.e.*, the catalyst site density of the CoPc|PVP-modified electrodes) used in this work is estimated using the relationship indicated in **eq S30**).

$$concentration\ of\ CoPc\ in\ PVP\ coating$$
$$= \frac{per-geometric\ area\ loading\ of\ CoPc\ deposited\ (nmol\ cm^{-2})}{film\ thickness\ of\ PVP\ coating\ (cm)}$$
$$= \frac{1.3\ nmol\ cm^{-2}}{5.22\ \times 10^{-4}\ cm} = 2.5\ \times\ 10^{-3}\ M$$

eq S30

Given the CoPc per-geometric area loading of 1.3 nmol cm^{-2} (see **Section 1.6 on Preparation of Electrode Coatings**) and the estimated PVI coating thickness of 4.4 μm (see **eq S29**), the concentration of CoPc in the PVI coatings (*i.e.*, the catalyst site density of the CoPc|PVI-modified electrodes) used in this work is estimated using the relationship indicated in **eq S31**.

$$concentration\ of\ CoPc\ in\ PVI\ coating = \frac{per-geometric\ area\ loading\ of\ CoPc\ deposited\ (nmol\ cm^{-2})}{film\ thickness\ of\ PVI\ coating\ (cm)} = \frac{1.3\ nmol\ cm^{-2}}{4.4\ \times 10^{-4}\ cm} = 3.0\ \times\ 10^{-3}\ M \quad \text{eq S31}$$

1.11 Estimations of the Ratios of Protonated to Freebase Sites and Apparent pK_a Values of the PVP and PVI Polymers

The acid-base chemistry of polyelectrolytes can significantly deviate from their monomeric counterparts.[22–24] Likewise, the pK_a of polyelectrolytes, such as PVP and PVI, demonstrate dependence on solution pH, as well as solution ionic strength and electrolyte salt identity. Thus, the apparent pK_a for ionizable polymers depends on the fraction of protonated sites on the polymer. Accounting for this variability in the apparent pK_a requires modification of the classic Hendersen-Hasselbalch equation[25–27] indicated in **eq S32**,

$$pH = pK_a - log(\frac{1\ -\ \alpha}{\alpha}), \quad \text{eq S32}$$

where $1-\alpha$ is fraction of protonated (*i.e.*, acidic) species and α is the fraction of deprotonated (*i.e.*, basic) species.

A modified version of the Hendersen-Hasselbalch equation[28] used for polyelectrolytes is given in **eq S33**,

$$pH = pK_{app\ (50\%)} - nlog(\frac{1\ -\ \alpha}{\alpha}), \quad \text{eq S33}$$

where p$K_{app\ (50\%)}$ is the apparent pK_a when the acid-base functional group of a polymer are present at 50% ionized and 50% non-ionized forms,[28,29] and n, is the polyelectrolyte parameter that accounts for electrostatic interactions between charged sites along the polymer backbone and ions in solution and is thus the slope of a pH vs $log(\frac{1\ -\ \alpha}{\alpha})$ plot.

Using values of p$K_{app\ (50\%)}$ (3.85 for PVP and 5.0 for PVI) and n (1.05 for PVP and 1.5 for PVI) taken from the literature,[30,31] **eq S31** enables approximating the ratio of protonated to deprotonated sites (*i.e.*, the value

$\frac{1-\alpha}{\alpha}$ of) within the PVP and PVI polymers at varying pH (see **Figure S8** and **Table S5**). The values of $\frac{1-\alpha}{\alpha}$ at varying pH also enable determination of the related apparent pK_a values at other fractions of ionized and non-ionized forms via leveraging the more classic Hendersen-Hasselbalch relationship given in **eq S32** and substituting the pK_a term for a pH dependent apparent pK_a (pK_{app}) as indicated in **eq S34**:

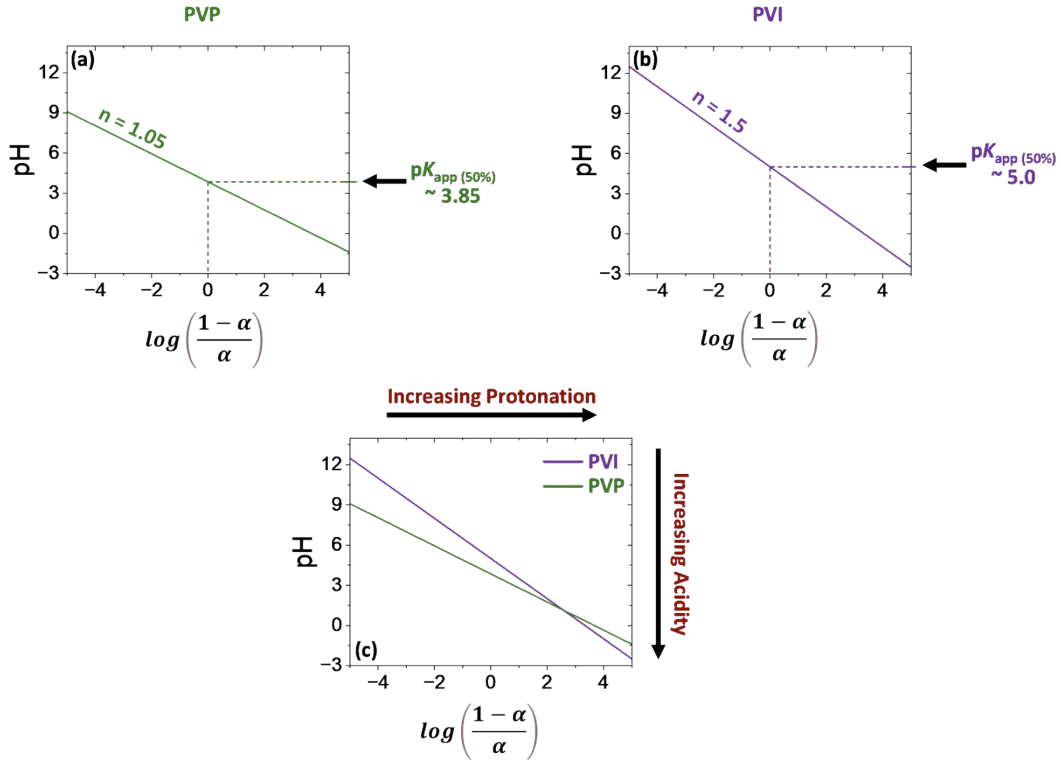

Figure S8. pH vs $log(\frac{1-\alpha}{\alpha})$ plots for **(a)** poly(4-vinylpyridine) (PVP), **(b)** poly(*N*-vinylimidazole) (PVI) and, for facilitating comparisons, **(c)** PVP and PVI. All plots were constructed using p$K_{app\ (50\%)}$ and n values obtained from literature reports, and were recorded in aqueous solutions at electrolyte concentrations near those used in the work reported herein (the reported values for PVP were determined using solutions containing 45% ethanol, 55% water and 0.05 M NaCl, and the reported values for PVI were determined using aqueous solutions containing 0.1 M NaCl).[28,30,31] In these plots, the slope of the line is equivalent to n, the polyelectrolyte parameter, a constant that represents the deviation from the classic Henderson-Hasselbalch relationship between pH, pK_a, and the degree of protonation (see eq S33 and eq S34).

$$pH = pK_{app} - log(\frac{1-\alpha}{\alpha}) \quad \text{eq S34}$$

Table S5. pK_{app}, $\frac{1-\alpha}{\alpha}$, % protonated, [N^+–H], and [N:] values for PVP and PVI at pH = 3.0, 4.7 and 6.7

Polymer	pH	pK_{app}	$\frac{1-\alpha}{\alpha}$	% Protonated[c]	[N^+–H] (M)	[N:] (M)
PVP[a]	3.0	3.81	6.45	86.6	8.03	1.24
	4.7	3.89	0.155	13.4	1.24	8.03
	6.7	3.99	0.00193	0.193	0.0179	9.26
PVI[b]	3.0	4.3	21	96	11	0.49
	4.7	4.9	1.6	61	6.8	4.3
	6.7	5.6	0.074	6.9	0.76	10

[a]The apparent pK_a when the acid-base functional group of a polymer are present at 50% ionized and 50% non-ionized forms, p$K_{app\ (50\%)}$, and the polyelectrolyte parameter that accounts for electrostatic interactions between charged sites along the polymer backbone and ions in solution, n, values for PVP (p$K_{app\ (50\%)}$ = 3.85, and n = 1.05) were taken from ref 29 (measured using solutions containing 0.05 M NaCl), and used to calculate the related values listed in this table.

[b]p$K_{app\ (50\%)}$ and n values for PVI (p$K_{app\ (50\%)}$ = 5.0, and n = 1.5) were taken from ref 30 (measured using solutions containing a 0.1 M NaCl) and used to calculate the related values listed in this table.

[c]% Protonated values are calculated using the relationship given in **eq S35**:

$$\%\ Protonated = (1-\alpha) \times\ 100. \qquad \text{eq S35}$$

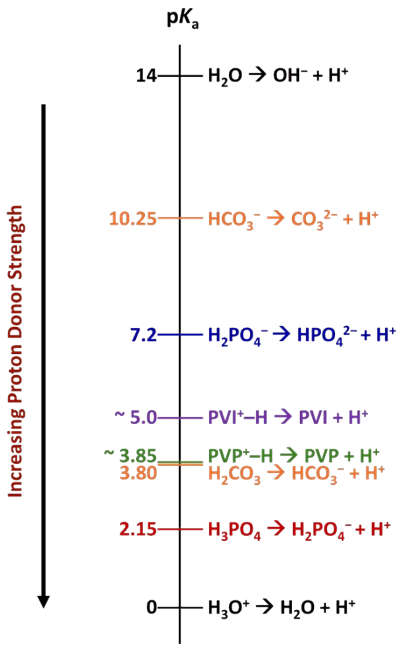

Figure S9. A diagram indicating pK_a values of the proton donors indicated in Figure 2 and water. For the "buffer-mediated" carbon dioxide reduction reactions indicated in Figure 2c of the main text, at standard state conditions, the pH of the solution is set by—and equal to—the pK_a of the proton donor, which influences the standard potential of the proton-coupled electron transfer reaction. In the case of polyelectrolytes such as PVP and PVI, the pK_a is an estimate of the apparent pK_a when the polymer is 50% protonated. The p$K_{app\ (50\%)}$ values of PVP and PVI used in this figure are taken from the literature and were recorded in aqueous solutions at electrolyte concentrations near those used in the work reported herein (the reported values for PVP were determined using solutions containing 45% ethanol, 55% water and 0.05 M NaCl, and the reported values for PVI were determined using aqueous solutions containing 0.1 M NaCl).[30,31] In the case of the acid-base chemistry involving phosphate and carbonate species, the indicated pK_a values[32,33] are where the solvent is water and are included to facilitate comparisons. For water, the total amount of carbonate in solution arising from sparging with 1 atm of CO_2 is <0.035 mol/L.[34] However, the ion concentration will perturb buffer ion activities. As examples, the pK_a of dihydrogen phosphate is ~6.81 in 0.1 M electrolyte, and ~6.67 in 0.4 M electrolyte, and ~6.62 in 1.0 M electrolyte. Unfortunately, the understanding of ions in solution is lacking as most theories pertain to dilute solutions yet physical situations with technological and biological relevance, are often not dilute.[35,36]

1.12 Faradaic Efficiency Calculations

As indicated in **eq S36**, the Faradaic efficiency (FE) is the ratio of the amount of chemical product ($N_{product}$) to the total amount of charge passed during the reaction (Q) multiplied by the Faraday constant (F) (96,485.3321 C mol^{-1}) and the number of electrons required to form the product (n).[37]

$$FE = \frac{N_{product}\,(mol) \times F\,(C\,mol^{-1}) \times n}{Q\,(C)}$$

eq S36

Table S6. Faradaic Efficiencies for CO (FE_{CO}) and H_2 (FE_{H2})

	FE_{CO} at pH = 4.7 (%)	FE_{CO} at pH = 3.0 (%)	FE_{H2} at pH = 3.0 (%)
CoPc|PVP	70	-	-
CoPc|PVI	81	16	71

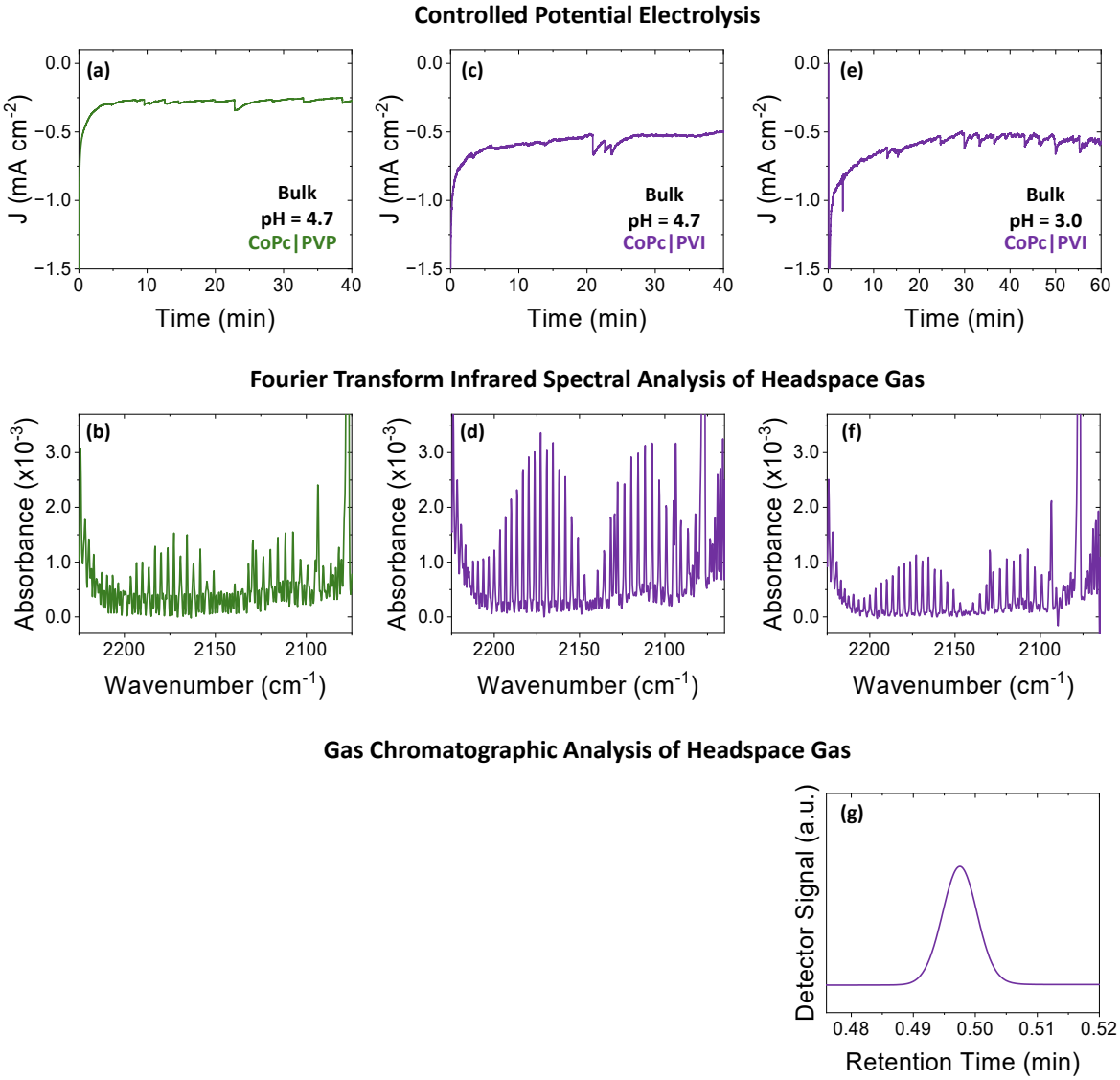

Figure S10. (a) A current-density vs time plot obtained via controlled-potential electrolysis experiments performed at an applied potential of -1.1 V vs SHE using a CoPc|PVP electrode suspended in 0.1 M NaH_2PO_4 at bulk pH = 4.7 and **(b)** a Fourier transform infrared spectrum of a headspace gas sample collected following 40 minutes of electrolysis at these conditions. **(c)** A current-density vs time plot obtained via controlled-potential electrolysis at -1.1 V vs SHE using a CoPc|PVI electrode suspended in 0.1 M NaH_2PO_4 at bulk pH = 4.7 and **(d)** Fourier transform infrared spectra of a headspace gas sample collected following 40 minutes of electrolysis at these conditions. **(e)** A current-density vs time plot obtained via controlled-potential electrolysis experiments performed at an applied potential of at -1.1 V vs SHE using a CoPc|PVI electrode suspended in 0.1 M NaH_2PO_4 at bulk pH = 3.0 and **(f)** a Fourier transform infrared spectrum of a headspace gas sample collected following 60 minutes of electrolysis at these conditions, as well as **(g)** a gas chromatogram of a headspace gas sample collected following 60 minutes of electrolysis.

1.13 Turnover Frequency Calculations

Given the total moles of CoPc units deposited onto all electrodes is 2.5 x 10^{-10} moles (see **Section 1.6 on the Preparation of Electrode Coatings** and **eq S17**), a potential-dependent turnover frequency, TOF_x, (where x indicates a TOF for either the production CO or H_2) can be determined using **eq S35**,[38,39]

$$TOF_x = \frac{N_{product}\,(mol)}{N_{cat}\,(mol)\ \times\ t\,(s)}, \qquad \text{eq S37}$$

where $N_{product}$ is the number of moles of chemical product produced (as determined by gas FTIR [for CO], or gas chromatograph [for H_2]), N_{cat}, is the number of moles of catalysts deposited onto the electrodes, and t is the duration of controlled potential electrolysis. In this expression, N_{cat} is taken as the total moles of CoPc deposited onto the electrodes (2.5 x 10^{-10} moles) (see **Section 1.6 on the Preparation of Electrode Coatings**), and $N_{product}$ is determined from the charge passed during controlled potential electrolysis as indicated in **eq S36**,

$$N_{product} = \frac{Q\,(C)\ \times\ FE_x}{n\ \times\ F\,(C\,mol^{-1})}, \qquad \text{eq S38}$$

where Q is the charge passed during controlled potential electrolysis, FE_x is the faradaic efficiency of gaseous product (CO or H_2) obtained from controlled potential electrolysis experiments (see **eq S36** and **Table S6**), and n is the number of electrons required to form the product (for the reduction of CO_2 to CO and H^+ to H_2 n = 2). Given this analysis uses the total loading of CoPc (including any that may be non-electroactive) and only account for product that is detected (and not any that may escape the electrochemical reaction cells), the TOF values reported herein are likely underestimated.

Table S7. Turnover Frequency for CO (TOF_{CO})

	TOF_{CO} at pH = 4.7 (s^{-1})	**TOF_{CO} at pH = 3.0 (s^{-1})**	**TOF_{H2} at pH = 3.0 (s^{-1})**
CoPc|PVP	0.83	-	-
CoPc|PVI	1.9	0.41	0.75

1.14 Determination of Means and Sample Standard Deviations

The mean ($\bar{x}$) and sample standard deviation (*s*; also known as estimated standard deviation) values reported in this article were obtained using **eq S39** and **eq S40**:[40,41]

$$\bar{x} = \frac{\sum x_i}{n'}$$

eq S39

$$s = \sqrt{\sum \frac{(x_i - \bar{x})^2}{n' - 1}}$$

eq S40

where *n'* is the total number of measurements (in this article, n = 3), and x_i is the observed value in the i_{th} measurement of *n'* total measurements (*i* = 1, 2, or 3). All values reported as means with sample standard deviations were determined from triplicate measurements of voltammograms recorded using three separately prepared samples of CoPc-PVP- or CoPc-PVI-GC electrodes.

1.15 Construction of Fitting Lines Using Unweighted Linear Regression

Linear fit plots were constructed using linear regression, where the slope and the intercept of the fitting line were determined by minimizing the sum of squares, *SS*, according to **eq S41**:[42]

$$SS = \sum w_j (y_j - (ax_j + b))^2, \quad \text{eq S41}$$

where x_j and y_j are the independent and dependent variables of a data set consisting of *m* data pairs (x_j, y_j), where *j* = 1, 2, ..., *m*. w_j is the weighting factor, *a* is the slope of the linear regression, and *b* is the y-intercept of the linear regression. Unless otherwise stated, w_j was set to 1, corresponding to no weighting.

2. Supplementary Figures, Equations, Tables, and Charts.

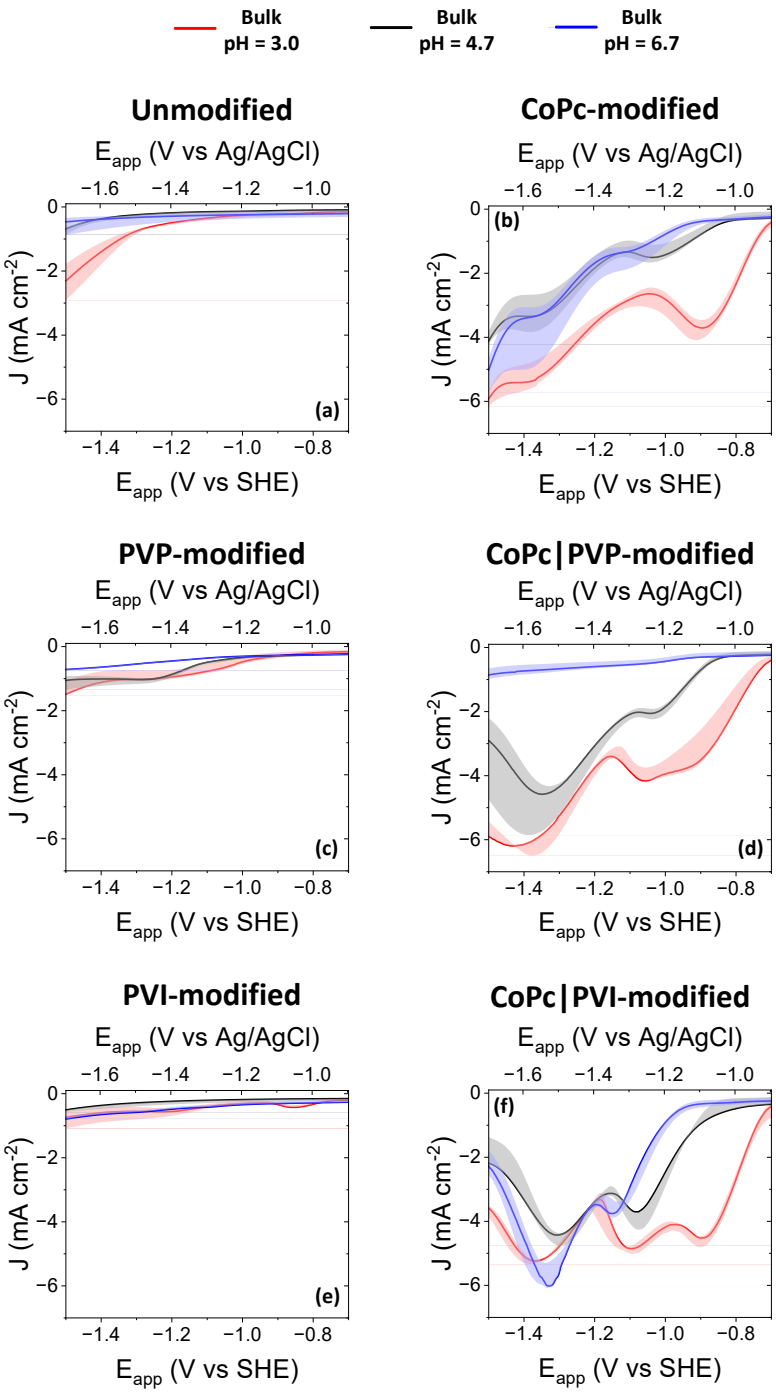

Figure S11. Voltammograms recorded at a scan rate of 200 mV s^{-1} using **(a)** unmodified glassy carbon working electrodes as well as electrodes modified with either **(b)** CoPc, **(c)** PVP, **(d)** CoPc|PVP, **(e)** PVI, or **(f)** CoPc|PVI. All data were recorded using 0.1 M NaH_2PO_4 solutions under CO_2 at a bulk pH = 3.0 (red), pH = 4.7 (black) or pH = 6.7 (blue). The shaded areas represent the standard deviations from the mean values.

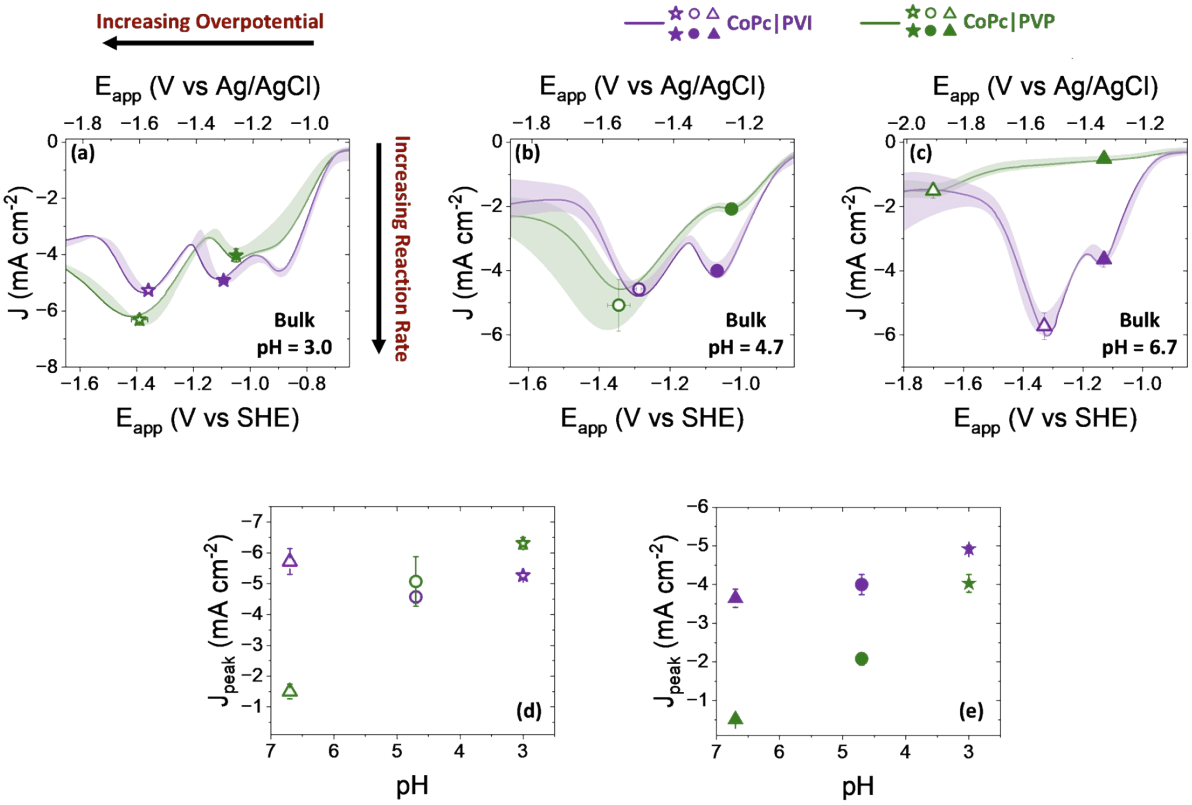

Figure S12. Voltammograms recorded at a scan rate of 200 mV s^{-1} using glassy carbon working electrodes modified with CoPc|PVP (green) or CoPc|PVI (purple), in 0.1 M NaH_2PO_4 solutions prepared to either **(a)** pH = 3.0, **(b)** pH = 4.7 or **(c)** pH = 6.7. **(d)** A plot of peak current density (J_{peak}) versus solution pH for the J_{peak} values proposed to arise from dihydrogen phosphate-mediated electrochemistry. **(e)** A plot of peak current density (J_{peak}) versus solution pH for the J_{peak} values proposed to arise from polymer-mediated electrochemistry. All voltammograms were collected under CO_2 (1 atm). The shaded areas and error bars represent the standard deviations from the mean values.

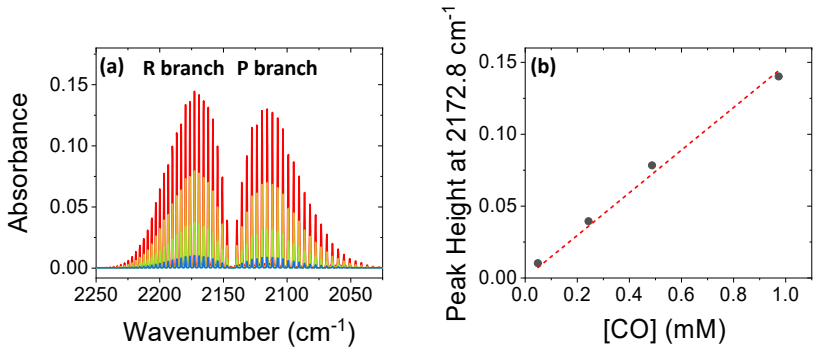

Figure S13. **(a)** Fourier transform infrared spectra of standard gas mixtures containing 1%, 5%, 10%, or 20% carbon monoxide (CO) in nitrogen gas (N_2) for preparation of **(b)** a calibration curve relating the height of the R branch peak at 2172.8 cm^{-1} versus CO concentration (in mM) used for quantification of CO in headspace gas samples collected following controlled potential electrolysis of CoPc-PVP or CoPc-PVI modified electrodes (see Figure S10).

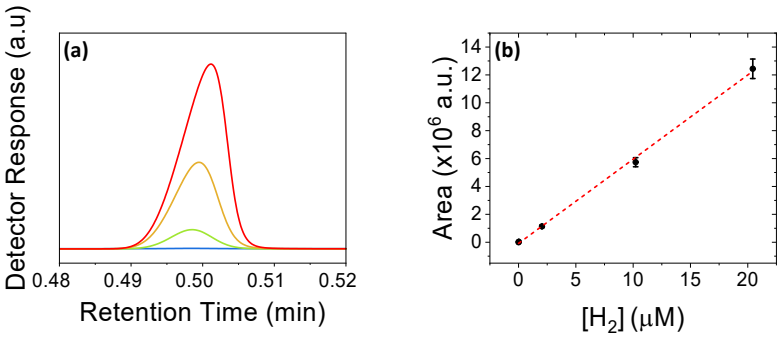

Figure S14. **(a)** Gas chromatographs of standard gas mixtures containing 0.01%, 1%, 5%, or 10% hydrogen (H_2) in nitrogen gas (N_2) for preparation of **(b)** a calibration curve relating the area under the H_2 signal curve to concentration (in μM) used for quantification of H_2 in headspace gas samples collected following controlled potential electrolysis of CoPc-PVI modified electrodes (see Figure S10).

3. Commentary on Donnan Potentials

Donnan potentials are electric potential differences ($\Delta\phi$) that form across membrane|solution interfaces when there are ions that cannot cross the interface and the non-diffusible charged species are present in different concentrations across the boundary of the respective phases. The imbalance of the non-diffusible charged species and the requirement for electroneutrality result in an unequal distribution of diffusible ions across the phases and the resulting Donnan potential which maintains overall electroneutrality (see Scheme 2 in the main text).[43–47] The Donnan potentials thus give rise to exclusion of co-ions, possessing the same charge sign as the non-diffusible species (Donnan exclusion), and inclusion of counter-ions, possessing the opposite charge sign as the non-diffusible species (Donnan inclusion).[43–45,48] When one of the diffusible species is a hydrogen ion (*i.e.*, H^+), this can give rise to a difference in the solution potential for hydrogen [abbreviated as pH and defined as a logarithmic scale that indicates the concentration of H^+ arising from changes in proton activity ($a_{H^+}^{sol}$) as indicated in equation S42],

$$pH = -\log_{10} a_{H^+}^{sol} = -\log_{10}\left(\gamma_{H^+}^{sol}\frac{C_{H^+}^{sol}}{c^\circ}\right) \quad \text{(the pH of a solution)} \qquad \text{(S42)}$$

In equation S42, $\gamma_{H^+}^{sol}$ is the chemical activity coefficient of protons in the solution phase (a dimensionless quantity that is the ratio of the chemical activity to the molar concentration), $C_{H^+}^{sol}$ is the concentration of protons in the solution phase (with units of mol L^{-1} and defined as moles of a species (H^+) as a solute per unit volume of the solution), and c° is the standard concentration, 1 mol L^{-1} (defined as moles of a solute per unit volume of the solution selected as a standard for reference). Although phenomena resulting from Donnan equilibria are often referenced with regards to biological functions[49–56] and some technological processes[57–60] they have been relatively underexplored in human-engineered materials involving electrocatalysis within polymeric coatings, which may provide strategies for controlling substrate and product concentrations at electrified interfaces.

4. Supplementary References

1. C. Chai and W. L. F. Armarego, *Purification of Laboratory Chemicals*, Butterworth-Heinemann, 5th edn., 2003.
2. T. J. Smith and K. J. Stevenson, *Handbook of Electrochemistry: 4-Reference Electrodes*, Elsevier B.V., 2007.
3. R. W. Ramette, *J. Chem. Educ.*, 1987, **64**, 885.
4. H. A. Dinçer, A. Koca, A. Gül and M. B. Koçak, *Dyes Pigm.*, 2008, **76**, 825–831.
5. F. Bedioui, E. De Boysson, J. Devynck and K. J. Balkus, *J. Electroanal. Chem. Interfacial Electrochem.*, 1991, **315**, 313–318.
6. B. R. Kozub and R. G. Compton, *Sens. Actuators B Chem.*, 2010, **147**, 350–358.
7. Y. Liu and C. C. L. McCrory, *Nat. Commun.*, 2019, **10**, 1683.
8. H. Hess, *Annalen der Physic*, 1840, **126**, 385–404.
9. T. L. Soucy, Y. Liu, J. B. Eisenberg and C. C. L. McCrory, *ACS Appl. Energy Mater.*, 2022, **5**, 159–169.

10. T. L. Soucy, W. S. Dean, K. E. Rivera Cruz, J. B. Eisenberg, L. Shi and C. C. L. McCrory, *J. Phys. Chem. C*, 2023, **127**, 14041–14052.
11. M. Wang, K. Torbensen, D. Salvatore, S. Ren, D. Joulié, F. Dumoulin, D. Mendoza, B. Lassalle-Kaiser, U. Işci, C. P. Berlinguette and M. Robert, *Nat. Commun.*, **10**, 3602.
12. W. W. Kramer and C. C. L. McCrory, *Chem. Sci.*, 2016, **7**, 2506–2515.
13. T. Shimomura, N. Oyama and F. C. Anson, *J. Electroanal. Chem.*, 1980, **112**, 265–270.
14. T. Yoshida, K. Kamato, M. Tsukamoto, T. Iida, D. Schlettwein, D. Wöhrle and M. Kaneko, *J. Electroanal. Chem.*, 1995, **385**, 209–225.
15. T. Abe, T. Yoshida, S. Tokita, F. Taguchi, H. Imaya and M. Kaneko, *J. Electroanal. Chem.*, 1996, **412**, 125–132.
16. X. Zhang, Z. Wu, X. Zhang, L. Li, Y. Li, H. Xu, X. Li, X. Yu, Z. Zhang, Y. Liang and H. Wang, *Nat. Commun.*, 2017, **8**, 14675.
17. H. Kang, A. Staples-West, A. Washington, C. Turchiano, A. Cooksy, J. Huang and J. Gu, *ChemCatChem*, 2023, **15**, e202300576.
18. ChemicalBook, https://www.chemicalbook.com/ChemicalProductProperty_EN_CB8406110.htm (Accessed 8-25-2025)
19. A. Loxley and B. Vincent, *Colloid Polym. Sci.*, 1997, **275**, 1108–1114.
20. M. J. Molina, M. R. Gómez-Antón and I. F. Piérola, *Macromol. Chem. Phys.*, 2002, **203**, 2075–2082.
21. M. J. Molina, M. R. Gómez-Antón and I. F. Piérola, *J. Phys. Chem. B*, 2007, **111**, 12066–12074.
22. R. M. Fuoss and U. P. Strauss, *J. Polym. Sci.*, 1948, **3**, 246–263.
23. A. V. Dobrynin and M. Rubinstein, *Prog. Polym. Sci.*, 2005, **30**, 1049–1118.
24. N. L. Mazyar, V. V Annenkov, V. A. Kruglova, S. M. Anan´ev, E. N. Danilovtseva, A. V Rokhin and S. V Zinchenko, *Izvestiya Akademii Nauk. Seriya Khimicheskaya*, 2000, **49**, 2013–2017.
25. J. Henderson, *Am. J. Phys.*, 1908, **21**, 173–179.
26. K. A. Hasselbalch, *Biochem. Z*, 1917, **78**, 112–144.
27. H. N. Po and N. M. Senozan, *J. Chem. Educ.*, 2001, **78**, 1499–1503.
28. A. Katchalsky and P. Spitnik, *J. Polym. Sci.*, 1947, **2**, 432–446.
29. A. M. Mika and R. F. Childs, *J. Membr. Sci.*, 1999, **152**, 129-140.
30. Y. E. Kirsh, O. P. Komarova and G. M. Lukovkin, *Eur. Polym. J.*, 1973, **9**, 1405–1415.
31. B. Popping, A. Deratani, B. Sebille, N. Desbois, J. M. Lamarche and A. Foissy, *Colloids and Surfaces*, 1992, **64**, 125–133.
32. R. N. Goldberg, N. Kishore and R. M. Lennen, *J. Phys. Chem. Ref. Data*, 2002, **31**, 231–370.
33. R. A. Kohn and T. F. Dunlap, *J. Anim. Sci.*, 1998, **76**, 1702–1709.
34. H. Zhong, K. Fujii, Y. Nakano and F. Jin, *J. Phys. Chem. C*, 2015, **119**, 55–61.
35. A. A. Green, *J. Am. Chem. Soc.*, 1933, **55**, 2331–2336.
36. T. Huang, S. M. Sarhangi, S. Granick and D. V. Matyushov, *Phys. Rev. Lett.*, 2025, **135**, 028002.
37. Z. Chen, T. F. Jaramillo, T. G. Deutsch, A. Kleiman-Shwarsctein, A. J. Forman, N. Gaillard, R. Garland, K. Takanabe, C. Heske, M. Sunkara, E. W. McFarland, K. Domen, E. L. Milled and H. N. Dinh, *J. Mater. Res.*, 2010, **25**, 3–16.
38. V. Artero and J. M. Savéant, *Energy Environ. Sci.*, 2014, **7**, 3808–3814.
39. C. Costentin, S. Drouet, M. Robert and J. M. Savéant, *J. Am. Chem. Soc.*, 2012, **134**, 11235–11242.
40. A. D. Wilkinson and A. McNaught, *IUPAC Compendium of Chemical Terminology*, International Union of Pure and Applied Chemistry, 3rd edn., 2019.
41. L. A. Currie and G. Svehla, *Pure & Appl. Chem.*, 1994, **66**, 595–608.
42. A. M. Almeida, M. M. Castel-Branco and A. C. Falcão, *J. Chromatogr. B: Anal. Technol. Biomed. Life Sci.*, 2002, **774**, 215–222.
43. W. Gaieck, A. Zhang, A. Sabatose, M. Ngo, E. Schwartz, W. White, S. Luo, L. Schulte, Y. Wang and S. Ardo, Teaching the concepts of Donnan potential and liquid-junction potential by evaluating homemade pH and ion-sensitive probes constructed using commercial ion-exchange membranes and reference electrodes. *ChemRxiv*. 2024, preprint, DOI:10.26434/chemrxiv-2024-hxgnv.

44. P. Aydogan Gokturk, R. Sujanani, J. Qian, Y. Wang, L. E. Katz, B. D. Freeman and E. J. Crumlin, *Nat. Commun.*, 2022, **13**, 5880.
45. Y. Tanaka, in *Ion Exchange Membranes*, Elsevier, 2015, pp. 29–65.
46. S. W. Boettcher, S. Z. Oener, M. C. Lonergan, Y. Surendranath, S. Ardo, C. Brozek and P. A. Kempler, *ACS Energy Lett.*, 2021, **6**, 261–266.
47. F. G. Donnan, *Chem. Rev.*, 1924, **1**, 73–90.
48. W. J. Koros, Y. H. Ma and T. Shimidzu, Terminology for membranes and membrane processes (IUPAC Recommendations 1996), *Pure and Applied Chemistry*, 1996, **68**, 1479–1489.
49. S. Kurbel, *J. Theor. Biol.*, 2008, **252**, 769–772.
50. W. W. Mapleson, *J. Pharmacol. Methods*, 1987, **17**, 231–242.
51. T. Goto, T. Hirabayashi, H. Morimoto, K. Yamazaki, N. Inoue, H. Matsuyama and I. Yumoto, *J. Bioenerg. Biomembr.*, 2016, **48**, 87–96.
52. E. Goulbourne, M. Matin, E. Zychlinsky and A. Matin, *J. Bacteriol.*, 1986, **166**, 59–65.
53. D. W. Jung, M. H. Davis and G. P. Brierley, *Arch. Biochem. Biophys.*, 1988, **263**, 19–28.
54. T. A. Krulwich, G. Sachs and E. Padan, *Nat. Rev. Microbio.l*, 2011, **9**, 330–343.
55. G. R. Bolton, A. W. Boesch, J. Basha, D. P. LaCasse, B. D. Kelley and H. Acharya, *Biotechnol. Prog.*, 2011, **27**, 140–152.
56. J. E. Langridge-Smith and W. P. Dubinsky, *J. Membr. Biol.*, 1986, **94**, 197–204.
57. V. Triandafilidi, S. G. Hatzikiriakos and J. Rottler, *Soft Matter*, 2018, **14**, 6222–6229.
58. M. Vis, R. Tuinier, B. W. M. Kuipers, A. Vrij and A. P. Philipse, *Soft Matter*, 2018, **14**, 4702–4710.
59. M. Vis, V. F. D. Peters, R. H. Tromp and B. H. Erné, *Langmuir*, 2014, **30**, 5755–5762.
60. R. M. Wallace, *Ind. Eng. Chem. Process Des. Dev.*, 1967, **6**, 423–431